1988

Low-temperature neutron powder diffraction study of chromium dioxide and the validity of the Jahn-Teller viewpoint

Jeremy K. Burdett, *University of Chicago*
Gordon J. Miller, *University of Chicago*
James W. Richardson, *Argonne National Laboratory*
Joseph V. Smith, *University of Chicago*

without oxalate must be involved in rapid preequilibrium but only the oxalate-containing complex undergoes the redox reaction between coordinated dioxygen and oxalate, as indicated by the following.

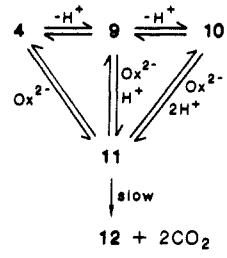

A more detailed picture of the reaction mechanism is illustrated in Scheme I. The proposed route for electron transfer is through the metal ions, which have low-energy orbitals capable of accepting the electrons, thus providing pathways for the electron-transfer process. Direct electron transfer from oxalate to peroxide is not considered likely because of their negative charges, leading to coulombic repulsions, which would space them far apart in the macrocyclic complex.

Further work in progress on this redox system is being directed toward obtaining structural information on the binary dioxygen-reducing substrate complex and toward the investigation of the reactions of other substrates capable of acting as bridging donors in the binuclear dicobalt-BISDIEN complex and in complexes of other binucleating macrocyclic ligands.

Acknowledgment. We express our thanks and appreciation to The Robert A. Welch Foundation for support of this research under Grant No. A-259 and to the donors of the Petroleum Research Fund, administered by the American Chemical Society.

Low-Temperature Neutron Powder Diffraction Study of CrO_2 and the Validity of the Jahn–Teller Viewpoint

Jeremy K. Burdett,*[†,§] Gordon J. Miller,[†,§] James W. Richardson, Jr.,[∥] and Joseph V. Smith*[‡,§]

Contribution from the Departments of Chemistry and Geophysical Sciences, The James Franck Institute, and Materials Research Laboratory, The University of Chicago, Chicago, Illinois 60637, and The Intense Pulsed Neutron Source, Argonne National Laboratory, Argonne, Illinois 60439. *Received March 21, 1988*

Abstract: The structure of CrO_2 has been determined at 10, 173, and 295 K by powder neutron diffraction. The structure of this material is interesting because the mode of distortion around the metal center is the reverse of that expected on the basis of local Jahn–Teller considerations. Band-structure calculations however, show that although the structure with two long and four short metal–oxygen distances is that expected for the d^0 configuration, where O–O repulsions control the picture, the opposite distortion is predicted for d counts leading to "t_{2g}" block degeneracies. We explain this result by constructing the d band dispersion curve using the angular overlap model. It is shown how through-bond coupling in the lower than octahedral local environment allows mixing between a component of each of the "e_g" and t_{2g} orbital sets and frustrates the energetic preferences predicted for the t_{2g} block alone. The factors that control the details of the geometries of the transition-metal oxides and fluorides with the rutile structure are explored.

The Jahn–Teller theorem[1] has enjoyed widespread use as a means of understanding the geometries of a variety of structures arising from a distortion of a symmetrical configuration of atoms.[2-4] According to the theorem the presence of an orbitally degenerate electronic state in a nonlinear molecule signals a geometrical instability. This may be relieved by a distortion whose symmetry species is contained within the antisymmetric direct product of the state symmetry. Such instabilities will naturally only be associated with highly symmetrical molecules. Octahedrally coordinated transition-metal complexes are particularly well-studied examples. Such orbitally degenerate states occur as the result of asymmetric occupation by electrons of degenerate orbitals.[5] The e_g^3 configuration of octahedral Cu^{II} is a classic example. Here, the distortion route associated with the ^2E_g electronic state is one of e_g symmetry. One component of a stretching motion of e_g symmetry, which will be useful to us, is shown in **1** and **2**. These represent different phases of a motion that describes the bulk of the observed distortions in these octahedrally derived structures.

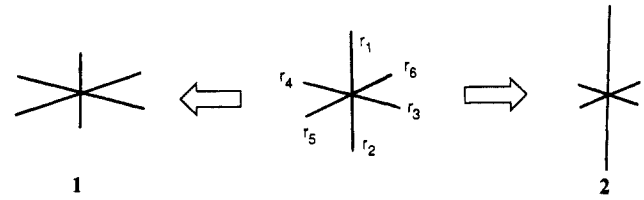

1 **2**

Even if the levels are not exactly degenerate, a second-order Jahn–Teller effect, accessible by perturbation theory,[4,6] often suffices to allow them to mix on distortion and lead to a stabilization of the system. The geometries of many transition-metal

[†] Department of Chemistry and The James Franck Institute, The University of Chicago.
[‡] Department of Geophysical Sciences, The University of Chicago.
[§] Materials Research Laboratory, The University of Chicago.
[∥] The Intense Pulsed Neutron Source, Argonne National Laboratory.

(1) (a) Jahn, H. A.; Teller, E. *Proc. R. Soc. London, A* **1937**, *161*, 220. (b) Jahn, H. A., *Ibid.* **1938**, *164*, 117.
(2) See almost any modern inorganic chemistry text. For a discussion by one of the originators of these ideas, see: Orgel, L. E. *An Introduction to Transition Metal Chemistry*; Methuen: London, 1960.
(3) Gazo, J.; Bersuker, I. B.; Garaj, J.; Kabesova, M.; Kohout, J.; Langfelderova, H.; Melnik, M.; Serator, M.; Valach, V. *Coord. Chem. Rev.* **1976**, *19*, 253.
(4) Burdett, J. K. *Molecular Shapes*; Wiley: New York, 1980.
(5) Not always does such a configuration give rise to a degenerate electronic state. In cyclobutadiene the $(e_g)^2$ configuration of the square geometry gives rise to a $^1B_{2g}$ ground state. The distortion of this molecule strictly arises via a pseudo-Jahn–Teller effect through a second-order term in the expansion of the energy in a perturbation sense along the distortion coordinate.[4,6]
(6) Bartell, L. S. *J. Chem. Educ.* **1968**, *45*, 754.

0002-7863/88/1510-8064$01.50/0

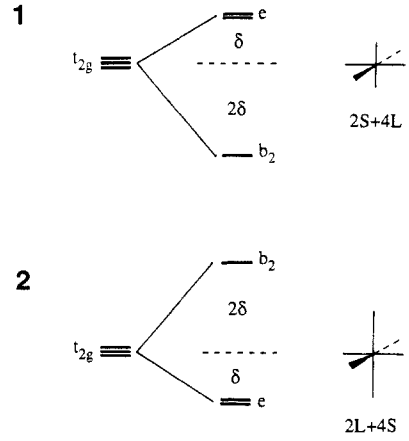

Figure 1. Splitting of the t_{2g} levels of a regular octahedral complex under the two tetragonal distortions, **1** and **2**.

and main-group molecules have been studied[4,7] by the perturbational aspect of the approach, even though the phrase second-order Jahn–Teller has often not been used. In lower symmetry situations, use of the angular overlap model has also been useful[8] in understanding the observed distortion route. In this paper we report the first low-temperature (10 K) structural determination of CrO_2, a system that distorts away from the octahedral geometry in the opposite direction to that predicted by simple application of molecular orbital ideas. We will show that one must be cautious in applying results derived from isolated molecules directly to the solid state without any consideration of the often significant dispersion effects, which may change the simple picture.

Predictions of Molecular Geometry Using the Angular Overlap Model. Jahn–Teller distortions of molecules are commonly separated into two categories:[4] (a) the first category is a strong effect involving occupation of metal–ligand σ^* levels (the e_g set in octahedral transition-metal complexes). Such distortions are usually static in nature, as seen from the well-studied examples of d^9 Cu(II) complexes. Most of these systems exhibit tetragonally distorted octahedra with two long and four short bonds (**2**). In the case of low-spin Ni^{II}, Pd^{II}, and Pt^{II}, the distortion is so large that square-planar complexes are universally observed. (b) The second category is a smaller effect, which is normally associated with asymmetric occupation of σ nonbonding, but π bonding or antibonding orbitals (the t_{2g} set in transition-metal complexes). At higher temperatures the effect is often a dynamic one with large oscillations about an equilibrium position. At lower temperatures, the structural distortion can be frozen out as seen in the low-spin d^5 $V(CO)_6$ species. This is found as a distorted octahedral molecule with two short (1.993 (2) Å) and four long (2.005 (2) Å) V–C distances.[9] The feature that distinguishes the static and dynamic aspects of (a) and (b) is simply the relative energetic importance of σ versus π interactions.

One of the aspects of the Jahn–Teller theorem that continues to attract interest is the prediction of the distortion route away from octahedral (**1** or **2**) as a function of the nature of the complex. In other words we wonder if there will be two short and four long (2S + 4L) or two long and four short (2L + 4S) distances. This may readily be examined theoretically as a function of d count. Here, we will use the ideas of the angular overlap model.[4] The energy changes associated with the (largely) transition-metal d orbitals for the case of π donor ligands (e.g. O) are shown in Figure 1 for the two distortions **1** and **2**. From our knowledge of the shapes of the three t_{2g} and two e_g orbitals, we can quantitatively follow how the two level patterns emerge. The form of one of the e_g distortion components, which describes **1** and **2**, is simply written as in eq 1. Here, the Δr_i's are the changes in the six bond

$$\Delta R = (2\sqrt{3})^{-1}(2\Delta r_1 + 2\Delta r_2 - \Delta r_3 - \Delta r_4 - \Delta r_5 - \Delta r_6) \quad (1)$$

(7) Burdett, J. K. *Struct. Bonding (Berlin)* **1976**, *31*, 67.
(8) Burdett, J. K. *Inorg. Chem.* **1981**, *20*, 1959.
(9) Bellard, S.; Rubinson, K. A.; Sheldrick, G. M. *Acta Crystallogr.* **1979**, *B35*, 271.

Table I. Total d Orbital Energies for the t_{2g} Configurations of the Regular, Tetragonally Compressed, and Tetragonally Elongated Octahedra[a]

d^n	regular	2S + 4L (**1**)	2L + 4S (**2**)
d^0	0	0	0
d^1	$4e_\pi$	$4e_\pi - 2\delta^*$	$4e_\pi - \delta$
d^2 (ls)[b]	$8e_\pi$	$8e_\pi - 4\delta^*$	$8e_\pi - 2\delta$
d^2 (hs)	$8e_\pi$	$8e_\pi - \delta$	$8e_\pi - 2\delta^*$
d^3 (ls)	$12e_\pi$	$12e_\pi - 3\delta$	$12e_\pi - 3\delta$
d^3 (hs)	$12e_\pi$	$12e_\pi$	$12e_\pi$
d^4 (ls)	$16e_\pi$	$16e_\pi - 2\delta$	$16e_\pi - 4\delta^*$
d_4 (is)	$16e_\pi$	$16e_\pi - 2\delta^*$	$16e_\pi - \delta$
d^5	$20e_\pi$	$20e_\pi - \delta$	$20e_\pi - 2\delta^*$
d^6	$24e_\pi$	$24e_\pi$	$24e_\pi$

[a] The asterisk indicates the lowest energy structure for π-donor ligands. [b] ls = low spin, hs = high spin, is = intermediate spin.

lengths around the octahedron. The distortions **1** and **2** differ only in the sign of the Δr_i. The angular overlap model allows expression of the molecular orbital energies in terms of parameters that measure the sizes of the various interactions present. The e_λ parameters measure the strength of the interaction between (for σ) a ligand σ orbital located along z with the z^2 orbital and (for π) a ligand π orbital, along x for example, with xz. The total interaction may be simply written in terms of these parameters coupled with trigonometric functions, set by the spherical harmonics, to describe the angular dependence. The e_λ parameters decrease in size with increasing metal–ligand distance. This may be modeled by writing $e_{\lambda'} = e_\lambda + \delta$, where δ accommodates the change in the parameter with distance. When this approach is used, at the regular octahedral geometry the t_{2g} energy levels are destabilized via M–O π^* interactions by $4e_\pi$ relative to the d orbital energy for the free atom, and the e_g levels are destabilized via M–O σ^* interactions by $3e_\sigma$. If we maintain these values as "centers of gravity", then on distortion, for the t_{2g} set, the b_2 orbital moves by 2δ in energy while the e pair move by $-\delta$. We have assumed here that the changes in e_λ are directly proportional to the change of distance in eq 1, shorter distances giving rise to larger e_λ values. Since $e_\pi > 0$, this implies that $\delta <$ for **1** and $\delta > 0$ for **2**. For case **1**, the b_2 orbital has a smaller M–O π overlap than in the octahedral structure and now lies at $4e_\pi - 2|\delta|$. The increased M–O π overlap with the two trans ligands on distortion destabilizes the e set, and they lie at $4e_\pi + |\delta|$. For case **2**, the opposite effect ensues; the b_2 orbital rises to $4e_\pi + 2|\delta|$, and the e levels fall to $4e_\pi - |\delta|$. A similar argument applies to the orbitals of the octahedral e_g set. Here, we use a parameter δ' to describe the variation in σ interaction. Notice that the splitting pattern here does not depend upon the distortion mode.

We shall be interested in the predictions of the model of the preferred distortion route as a function of d count, but note that a prediction is only possible for asymmetric t_{2g} configurations. For systems involving partial occupancy of the e_g orbitals, the model makes no prediction as to the preferred route. In fact, we have to look at the effect of d–s mixing via the second-order Jahn–Teller effect[4,8,10] to understand the virtually universal occurrence of **2** in the chemistry of Cu^{II}, for example.

Table I shows the d orbital energies of all relevant t_{2g} configurations for the octahedral structure, for **1** and for **2**. This tabulation clearly indicates that the electronically controlled distortion mode to **1** or **2** is configuration dependent. (Parenthetically, we note that, within the premises of the Jahn–Teller theorem, other distortions of T_{2g} and T_{1g} states are certainly possible to give structures containing 3-fold or 2-fold rotation axes.) Furthermore, interactions between ligands may also contribute to the observed geometry as discussed specifically for d^4 transition-metal complexes by Kubáček and Hoffmann.[11] The structure predicted to be most stable for π-donor ligands is indicated with an asterisk. The predictions are reversed if the ligands are π acceptors. Thus, for example, the distortion **1** found[9] for low-spin d^5 $V(CO)_6$ noted above is correctly predicted.

(10) Gerloch, M. *Inorg. Chem.* **1981**, *20*, 638.
(11) Kubáček, P.; Hoffmann, R. *J. Am. Chem. Soc.* **1981**, *103*, 4320.

Table II. Neutron Powder Diffraction Data and Structure Refinement for CrO_2

	X-ray[a]	neutron		
temp, K	295	295	173	10
space gp[b]	$P4_2/mnm$	$P4_2/mnm$	$P4_2/mnm$	$P4_2/mnm$
a_o, Å	4.4190 (3)	4.42193 (4)	4.41782 (4)	4.41632 (4)
c_o, Å	2.9154 (1)	2.91659 (4)	2.91697 (4)	2.91736 (4)
V, Å^3	56.930	57.029 (1)	56.931 (1)	56.900 (1)
ρ_x, g cm^{-3}	4.935	4.927	4.935	4.938
d_{min}, Å		0.398	0.398	0.398
d_{max}, Å		3.966	3.966	3.966
no. of reflctn used (triclinic)		1993	1961	1961
no. of param		24	24	25
R_{wp}, %		6.93	7.24	6.84
R_{exp}, %		4.80	4.85	3.93
R_{F^2}(nuclear), %		8.31	7.76	7.55
R_{F^2}(magnetic), %		15.02	12.43	11.86

[a] Reference 24. [b] $Z = 2$ for all four entries.

CrO_2 is isostructural with rutile[12] and is a high-spin d^2 system. No distortions apparently occur along the chain axis, which may be attributed to metal–metal bonding as found in the isoelectronic (but low-spin) systems MoO_2[13] and WO_2 as well as in d^1 VO_2 and d^3 α-ReO_2 and TcO_2. Here, the metal atoms pair up along the chain axis. For high-spin d^2 systems such as CrO_2, the preferred distortion predicted from Table I is that which produces two long and four short Cr–O distances (**2**), a prediction opposite to that observed[12] via X-ray crystallography.[14] In order to study this problem further, we have carried out an accurate redetermination of the structure of CrO_2 at room temperature and 173 and 10 K using the Intense Pulse Neutron Source (IPNS) at the Argonne National Laboratory. This structural investigation in complemented with band-structure calculations of the tight-binding type in order to understand the electronic effects controlling the distortion of the CrO_6 octahedra in the condensed phase. The study extends our recent work[15] on the two TiO_2 polymorphs, rutile and anatase.

Structural Determination

Diffraction Data Collection. A powedered sample of CrO_2, supplied by Dr. A. Sleight of E. I. Du Pont, was sealed in a cylindrical vanadium can ($^7/_{16}$-in. diameter, $2^1/_4$-in. length, 0.5-mm wall thickness) in a helium atmosphere and cooled by a two-stage, closed-cycle Displex refrigerator. Data were collected on the special-environment powder diffractometer[16] at IPNS at controlled temperatures of 295, 173, and 10 K. Diffraction data from the ±150° banks of detectors were fit by the Rietveld method[17] modified for time-of-flight neutron powder diffraction data.[18,19] Backgrounds were fit with a six-parameter analytical function. The resolution function defining the peak shapes of Bragg reflections is the convolution of a leading exponential, a lagging exponential, and a Gaussian.[20] The Gaussian width was varied during these refinements to account for anisotropic strain effects.

Table III. Atomic Positions and Anisotropic Displacements of CrO_2[a]

		X-ray	neutron		
		295 K	295 K	173 K	10 K
Cr	$x = y = z$	0	0	0	0
	$U_{11} = U_{22}$	0.0055 (2)	0.0046 (3)	0.0035 (3)	0.0025 (2)
	U_{33}	0.0042 (3)	0.0017 (4)	0.0001 (4)	0.0001 (3)
	U_{12}	0.0003 (2)	0.0004 (4)	0.0003 (4)	0.0003 (3)
	$U_{13} = U_{23}$	0	0	0	0
O	$x = y$	0.3026 (3)	0.30240 (8)	0.30226 (8)	0.30225 (8)
	z	0	0	0	0
	$U_{11} = U_{22}$	0.0068 (4)	0.0061 (2)	0.0048 (2)	0.0040 (1)
	U_{33}	0.0055 (6)	0.0044 (2)	0.0035 (2)	0.0027 (2)
	U_{12}	−0.0011 (6)	−0.0020 (2)	−0.0011 (2)	−0.0009 (2)
	$U_{13} = U_{23}$	0	0	0	0
	occupancy factor	1.0	1.014 (7)	1.027 (7)	1.020 (6)

[a] The general form for the temperature factor is $\exp[-2\pi^2(U_{11}h^2a^{*2} + \ldots + 2U_{23}klb^*c^*)]$.

Table IV. Interatomic Distances (Å) and Angles (deg) for CrO_2

		295 K	173 K	10 K
Cr–O	4×	1.9114 (3)	1.9114 (3)	1.9113 (3)
Cr–O′	2×	1.8911 (5)	1.8884 (5)	1.8877 (5)
O–Cr–O	2×	99.45 (2)	99.47 (2)	99.49 (2)
O–Cr–O	2×	80.55 (2)	80.53 (2)	80.51 (2)
O′–Cr–O′	2×	180.00	180.00	180.00
O–Cr–O′	4×	90.00	90.00	90.00
Cr–O–Cr	2×	130.28 (1)	130.27 (1)	130.25 (1)
Cr–O–Cr	1×	99.45 (2)	99.47 (2)	99.49 (2)

Anistropic Broadening. Individual fitting of the Bragg diffraction peaks revealed a distinct anisotropy in the peak widths, with greatest broadening in the (210) direction. This behavior is commonly found in CrO_2 samples, which have been treated to prevent hydrogen reduction to CrOOH[21,22] and is the result of occasional stacking faults along (210). The peak anisotropy is handled by the Rietveld refinement program by introducing additional terms to the Gaussian function, which produce broadening that is greatest in a chosen direction ((210) in this case) and decreases as $\cos^2 \chi(hkl)$, where $\chi(hkl)$ is the angle between (210) and the remaining reflections (hkl). In a tetragonal crystal system, the unique reflection set consists of half an octant, which is not sufficient to thoroughly describe the broadening effects observed. Hence, a triclinic set (one hemisphere), with symmetry-extinct reflections removed, was generated and used in the Rietveld refinements.

Magnetic Scattering. CrO_2, being a high-spin system, is ferromagnetic (0–400 K). Neutron diffraction experiments, therefore, will exhibit magnetic scattering from the Cr^{4+} ions. Ferromagnetic scattering results in additional intensity contributions to the subset of nuclear Bragg reflections to which the magnetic ions (Cr^{4+}) contribute; no superlattice reflections will be observed. Included in the Rietveld refinement was a calculation of the magnitude of the magnetic moment (μ) and the angle (ϕ) of the magnetic moment vector with respect to the c axis (complete directional information about the magnetic moment in a tetragonal system is not obtainable from a powder diffraction experiment[23]).

Rietveld Refinements. Rietveld refinements at 295, 173, and 10 K were carried out including refinement of lattice, background, atomic positional, atomic anisotropic displacement, anisotropic peak shape, extinction, and absorption parameters, along with the magnetic moment magnitude and direction. Pertinent data relating to data collection and structural refinement are presented in Table II. An additional column in this and subsequent tables represents room-temperature results from the most recently published single-crystal X-ray refinement,[24] for comparison with the neutron results. The profile fits for the Rietveld refinements are presented in Figure 2. Comparison of lattice parameters is important for assessing the effect of anisotropic broadening and the extent of reduction to β-CrOOH. As Table II indicates, the room-temperature neutron parameters are consistently higher than the single-crystal X-ray values by ~0.05% (the X-ray values may be biased by peak asymmetry from absorption). The volume of β-CrOOH (61.750 Å^3) is

(12) Cloud, W. H.; Schreiber, D. S.; Babcock, K. R. *J. Appl. Phys.* **1962**, *33*, 1193.
(13) Rogers, D. B.; Shannon, R. D.; Sleight, A. W.; Gillson, J. L. *Inorg. Chem.* **1969**, *8*, 841.
(14) For low-spin d^2 compounds, the other case is favored. However, with two short and four long M–O bonds, we have another Jahn–Teller instability (asymmetric occupation of the e level), and, therefore, a further distortion may ensue by breaking the 4-fold rotation axis.
(15) (a) Burdett, J. K.; Hughbanks, T.; Miller, G. J.; Richardson, J. W., Jr.; Smith, J. V. *J. Am. Chem. Soc.* **1987**, *109*, 3639. (b) Burdett, J. K. *Inorg. Chem.* **1985**, *24*, 2244.
(16) IPNS Progress Report; Argonne National Laboratory: Argonne, IL, 1981–1983.
(17) Rietveld, H. M. *J. Appl. Crystallogr.* **1969**, *2*, 65.
(18) Jorgensen, J. D.; Rotella, F. J. *J. Appl. Crystallogr.* **1982**, *15*, 27.
(19) Von Dreele, R. B.; Jorgensen, J. D.; Windsor, C. G. *J. Appl. Crystallogr.* **1982**, *15*, 581.
(20) Rotella, F. J. *Users Manual for Rietveld Analysis of Time-of-Flight Neutron Powder Diffraction Data at IPNS*; Argonne National Laboratory: Argonne, IL, 1986.
(21) Saez-Puche, R.; Alario-Franco, M. A. *J. Solid State Chem.* **1981**, *38*, 87, and references therein.
(22) Christensen, A. N.; Hansen, P.; Lehmann, M. S. *J. Solid State Chem.* **1976**, *19*, 299.
(23) Shirane, G. *Acta Crystallogr.* **1959**, *12*, 282.
(24) Prota, P.; Marezio, M.; Remeika, J. P.; Dernier, P. D. *Mater. Res. Bull.* **1972**, *7*, 157.

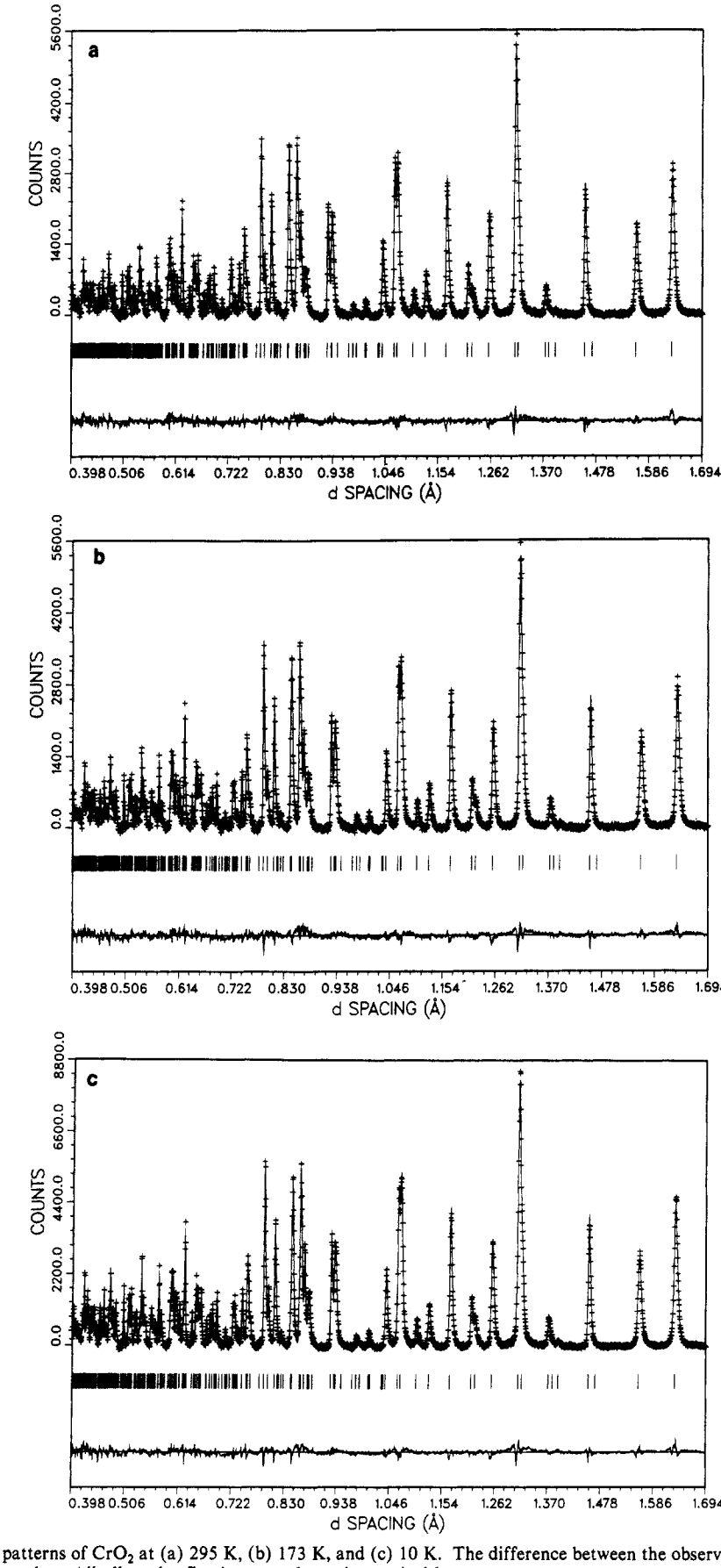

Figure 2. Neutron powder patterns of CrO_2 at (a) 295 K, (b) 173 K, and (c) 10 K. The difference between the observed data (+) and the calculated profile is shown by the lower plot. All allowed reflections are shown by vertical bars.

~8.5% larger than that of CrO_2 (56.931 Å^3 from X-ray refinement), and both $(a + b)/2$ and c are larger for β-CrOOH than for CrO_2. Although the neutron parameters are consistent with very slight reduction of CrO_2 to β-CrOOH, the values are within the rather wide range of reported values, and the discrepancies are not significantly larger than those observed for our neutron diffraction results for rutile TiO_2.[15] Siratoi and Iida observed that c increases with temperature from ~80 to 173 K and then decreases up to 473 K.[25] Unfortunately, we cannot compare this

Table V. Local Coordination in Transition-Metal Dioxides and Difluorides with Rutile-Type Structures (Distances in Å)

system	linkages: four	linkages: two	$r_2/r_4^a - 1$	distortion type
MgF_2	1.998	1.979	-	1
CrF_2	2.01,[b] 1.98	2.43	+	2
MnF_2	2.131	2.104	-	1
FeF_2	2.118	1.998	-	1
CoF_2	2.049	2.027	-	1
NiF_2	2.022	1.981	-	1
CuF_2	1.93[b]	2.27	+	2
ZnF_2	2.046	2.012	-	1
TiO_2	1.945	1.986	+	2
CrO_2	1.911	1.888	-	1
RuO_2	1.984	1.942	-	1
OsO_2	2.006	1.962	-	1

[a] The ratio of the 2-fold set of M–X distances to the 4-fold set, in the tetragonal structure. [b] Monoclinic structure. Three pairs of distances.

trend with our results, although we did find that c decreases from 10 to 173 K.

Atomic structural parameters are given in Table III. The neutron and X-ray values for x(O) at room temperature agree within experimental error. Comparison of the anisotropic displacement parameters reveals that the neutron values, although equal within experimental error (with the exception of U_{33}(Cr)), are systematically lower than the X-ray values. This can be expected when neutron and X-ray values are compared, due to the difference in the physical origin of the diffraction. In fact, the parameters for oxygen are viturally identical with the values we obtained for O in TiO_2 (U_{11} = 0.0057 (1), U_{33} = 0.0044 (1), U_{12} = −0.0019 (1) Å^2). Comparison of the parameters for Cr with those for Ti in TiO_2 (U_{11} = 0.0055 (2), U_{33} = 0.0045 (3), U_{12} = −0.0003 (3) Å^2) suggests that the anisotropy of the Cr sites is real. This anisotropy persists to 10 K. U_{33} for both Cr and O is lower than U_{11}. However, addition of a correction for preferred orientation to the room-temperature refinement, along the c direction, resulted in no significant improvement of the fit or change in the displacement parameters. As with TiO_2, the noticeable displacement of the oxygen atoms normal to the plane containing its three nearest neighbors, as evidenced by the rather large U_{12}, persists to 10 K.

Distances and angles are tabulated in Table IV. The Cr–O distances representing equatorial vertices in the octahedra remain virtually unchanged. There is a small change in the Cr–O′ (axial) distances, largely a result of the change in a. A consequence of this is very subtle increase in the distortion of the Cr octahedra.

Our magnetic scattering results (295 K, μ = 1.7 (3) μ_B, ϕ = 20°; 173 K, μ = 2.0 (3) μ_B, ϕ = 21°; 10 K, μ = 2.1 (2) μ_B, ϕ = 23°) are in reasonably good agreement with previously reported data (298 K, μ = 1.51 μ_B, $\phi \approx 20°$,[26] 78 K, μ = 1.97 μ_B, $\phi \approx 30°$,[26] 10 K, μ = 2.04–2.07 μ_B[27,28]). The increase in magnetic moment is expected as the spins become more perfectly aligned at temperatures further from the magnetic transition temperature.

Clearly the local details of the structure of CrO_2 are at variance with the simple molecular model we have used. However, the result is not confined to the oxides. Table V has collected bond length data for a series of rutile-type oxides and fluorides where there is no metal–metal dimer formation. Notice by comparison with Table I that, although the structure of FeF_2 is correctly predicted using Jahn-Teller ideas for an isolated octahedron, that of CoF_2 is not.

Energy Bands of the Solid

The failure of a molecular model to account for the distortion in solid CrO_2 and several of the other oxides and fluorides of Table V is, after a little thought, not very surprising. From our previous studies on transition-metal sulfides of the pentlandite type[29] and of others on the electronic structure of the edge-sharing tetrahedral chains[30] with stoichiometry FeS_2^-, the ligand field at transition-metal centers is significantly affected by the requirements of translational symmetry. Through-bond and through-space interactions are often both quite important. We therefore need to use a theoretical model that uses and the band structure of the solid. We first present results obtained via the extended Hückel model and then use the angular overlap model for direct comparison with the molecular case.

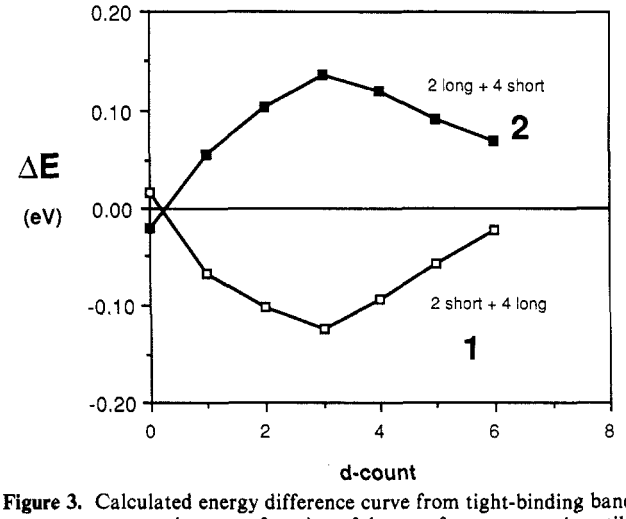

Figure 3. Calculated energy difference curve from tight-binding band-structure computations as a function of d count for a prototypic rutile-type oxide (TiO_2 itself was the system chosen) for the two tetragonal distortions, **1** and **2**.

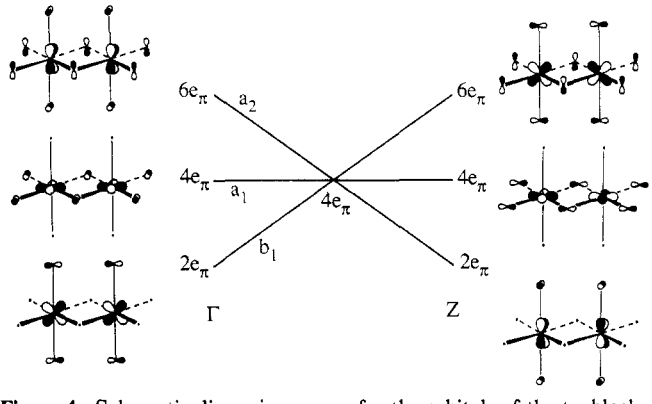

Figure 4. Schematic dispersion curves for the orbitals of the t_{2g} block along the line Γ to Z of the Brillouin zone. The angular overlap model with its units of e_π was used to construct the diagram.

There are, in fact, three diffeernt distortions noted in Table V. The rutile space group does not constrain the two sets of symmetry-inequivalent distances to be equal, and indeed none are. Distortions of the type **1** and **2**, which preserve the $P4_2/mnm$ space group, are represented here. Distortion of the M–X linkages along the chain gives rise to a much lower symmetry (monoclinic), and three different pairs of M–X distances are found. There are two examples of these, both associated with e_g orbital degeneracies, namely CuF_2 and CrF_2. Here, we shall be interested only in those distortions that preserve the tetragonal structure. (Elsewhere, we shall examine the factors promoting the monoclinic structure.) Figure 3 shows two energy differences curves, calculated using the extended Hückel method, as a function of d electron count for the two types of local distortions at the metal octahedra in rutile that preserve the space group. These results agree quite well with the observed structures for most transition-metal dioxides and difluorides with the rutile structure: the most prevalent distortion is the tetragonal compression of the octahedron (Table V), case **1**. The only exceptions occur for the d^0 configuration and the high-temperature tetragonal polymorph of VO_2. (Figure 3 shows curves for the low-spin d^n configurations. Within our one-electron framework the plots for high-spin systems are readily generated. For example, the values appropriate for high-spin d^2 are simply half of the energy differences calculated for low-spin d^4.) With reference to Table I, notice that the configuration

(25) Siratori, K.; Iida, S. *J. Phys. Soc. Jpn.* **1960**, *15*, 2362.
(26) Cloud, W. H.; Schreiber, D. S.; Babcock, K. R. *J. Appl. Phys.* **1962**, 33 (supplement), 1193.
(27) Guillaud, C.; Michel, A.; Bernard, J.; Fallot, M. *C. R. Hebd. Seances Acad. Sci.* **1944**, *219*, 58.
(28) Siratori, K.; Iida, S. *J. Phys. Soc. Jpn.* **1960**, *15*, 210.
(29) Burdett, J. K., Miller, G. J. *J. Am. Chem. Soc.* **1987**, *109*, 4081.
(30) Silvestre, J.; Hoffmann, R. *Inorg. Chem.* **1985**, *24*, 4108.

dependence of the molecular model is removed, suggesting that a first-order Jahn–Teller effect is not influencing the local geometry of the transition-metal center in these rutile phases. In the following discussion, we shall see that second-order, symmetry-allowed orbital mixing of a second-order Jahn–Teller type primarily contributes to the features of both curves.

We begin by using the angular overlap model to determine the energy levels of solid rutile. A good feeling for the energetics of these systems may be obtained by looking at the structure of a single edge-sharing octahedral chain. Figure 4 shows schematically how the intrachain M–O interactions split the t_{2g} levels along the line ΓZ in the tetragonal Brillouin zone. Metal–metal interactions are temporarily ignored. The energies are calculated with the angular overlap model, and the symmetry labels correspond to the point group C_{2v} for an isolated MX_4 chain, isomorphous to the group of any general point in the one-dimensional zone. Although we show a linear dispersion for both the b_1 and a_2 bands, the k dependence is strictly given by $\cos^2(ka/2)$. Note that, at the midpoint of the ΓZ line, $(0, 0, \pi/2c)$, all three bands are isoenergetic. This particular point is the mean-value point for the one-dimensional zone[31] and is useful for calculating average quantities of the entire zone for one-dimensional systems. When M–M bonding is turned on, within the angular overlap model approximation, this degeneracy remains because the orbitals at this point are rigorously M–M nonbonding.

Figure 5 shows the changes in the energy levels for the MX_4 chain at Γ, Z, and the mean-value point with the temporary restriction that no M–M interactions are included. The energy difference curves between the two distortions **1** and **2** and the octahedral geometry evaluated with the mean-value point are shown in **3**. The constraints on the angular overlap model pa-

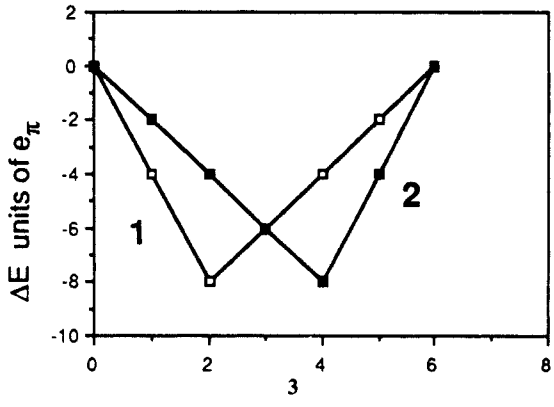

rameter (δ) are similar to those imposed for the isolated octahedral complexes in order to maintain an energetic center of gravity. In case **1**, (2S + 4L), the shortened M–O bonds are perpendicular to the chain axis and destabilize the $b_1(\Gamma)$ and $a_2(Z)$ levels, whose only oxide components come from the axial atoms. The lengthening of the M–O distances along the chain stabilizes the a_1 level at every point. The remaining $a_2(\Gamma)$ and $b_1(Z)$ levels are unchanged in energy due to the competition between the axial shrinkage and the longitudinal stretching. Again, opposite energetic trends occur for the other distortion. The structural preferences predicted from these simple energetic arguments are identical with those for the Jahn–Teller distorted octahedral molecule (Table I). The shapes of the two curves are very different from those of Figure 3, and indeed their predictions are badly in error. For example, we would predict the distortion **2** (2L + 4S) to be favored for low-spin d^4 systems, which is not observed for either RuO_2 or OsO_2. Neither would we predict distortion **1** for high-spin d^2, namely for CrO_2 itself. Futhermore, we do not obtain the relative extremum at d^3 found in Figure 4.

Figure 6 illustrates how these schemes are changed when M–M interactions are included. The labels ϵ_i are used here for metal–metal interactions. We note a redistribution of the energy levels

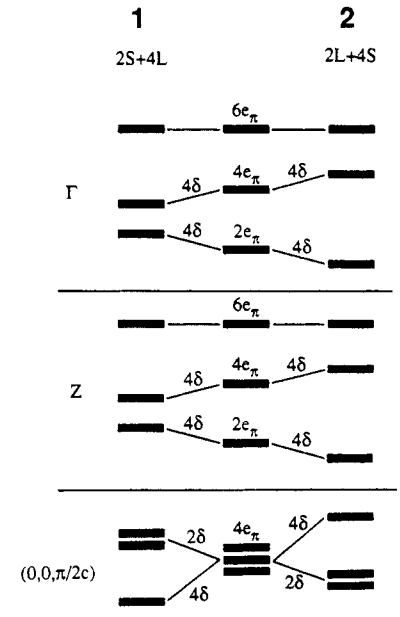

Figure 5. Orbital correlations for the three t_{2g} levels of Cr in CrO_2 with no metal–metal interactions included, at three pertinent points of the Brillouin zone. The parameter δ is the same as that used in Table I and Figure 1.

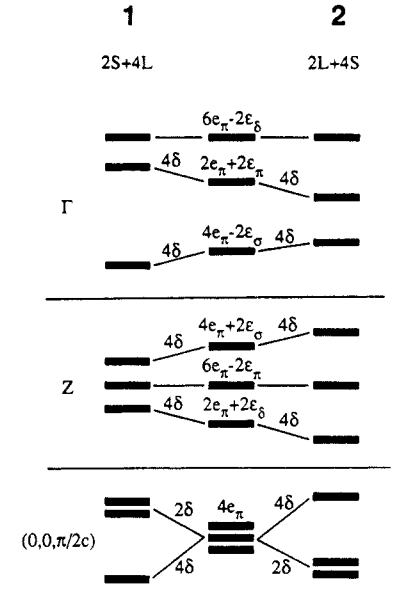

Figure 6. Orbital correlations for the three t_{2g} levels of Cr in CrO_2 with metal–metal interactions included, at three pertinent points of the Brillouin zone. The parameter δ is the same as that used in Table I and Figure 1, and the parameter ϵ_λ ($\lambda = \sigma, \pi, \delta$) measures the changes in the metal–metal interactions.

at the two high-symmetry points, but since the M–M interactions at the mean value point are strictly nonbonding, the same difference curve as in **3** results.

In our discussion thus far, we have not mentioned the e_g set of d orbitals because they are unoccupied for the d^2 CrO_2 as well as for d^4 RuO_2 and OsO_2 systems. Yet, one of these orbitals, the a_1 d_{z^2} orbital, is rather influential in the distortion energetics. We notice (**4**) that it has the same symmetry as one of the t_{2g} orbitals

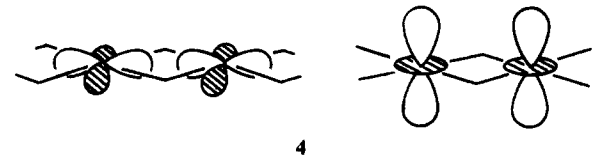

4

in the solid. Because the group of any general point in the one-dimensional zone is isomorphous to C_{2v}, in order to determine the

(31) (a) Chadi, D. J., Cohen, M. L. *Phys. Rev. B: Solid State* **1973**, *B7*, 5747. (b) Baldereschi, A. *Phys. Rev. B: Solid State* **1973**, *B7*, 5212.

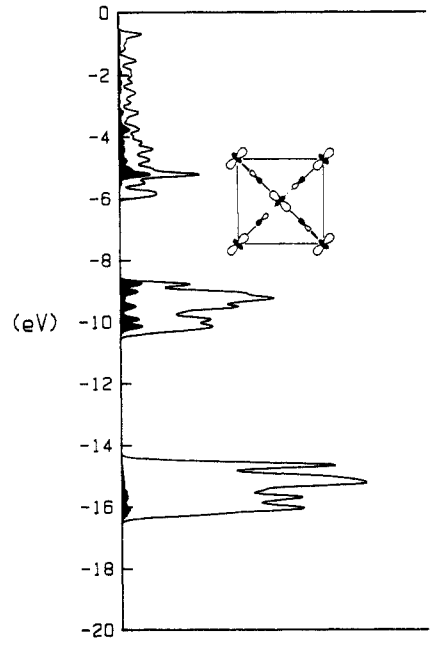

Figure 7. Total DOS for CrO_2 with the d_{z^2} orbital (one of the e_g set) projection shaded. Along the chain direction these orbitals transform as a_1.

energy levels for the a_1 e_g and a_1 t_{2g} orbitals here, we need to solve a secular determinant; i.e., these orbitals, orthogonal in the molecule, are now allowed by symmetry to interact with each other. From the ideas of perturbation theory we know these levels will repel each other so that the relevant t_{2g} orbital will be stabilized. It is straightforward to evaluate the stabilization energy as the quantity $\epsilon_{stab} \sim (4e_\pi e_\sigma)/(4e_\pi + 3e_\sigma)$. To estimate the magnitude of this energy, if we assume σ and π overlap integrals are related as $S_\pi \sim 0.25S_\sigma$, then $e_\pi \sim 0.06e_\sigma$ and $\epsilon_{stab} \sim 0.08e_\sigma$. This is a value on the order of e_π! This phenomenon is effective throughout the Brillouin zone. **5** shows shows how Figure 4 is

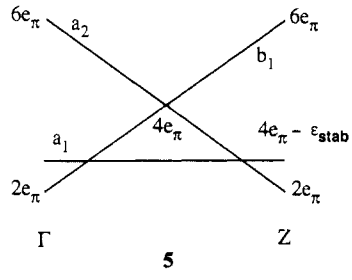

5

modified. The energy difference curves for the two distortions are readily calculated on the new scheme and are shown in **6** with

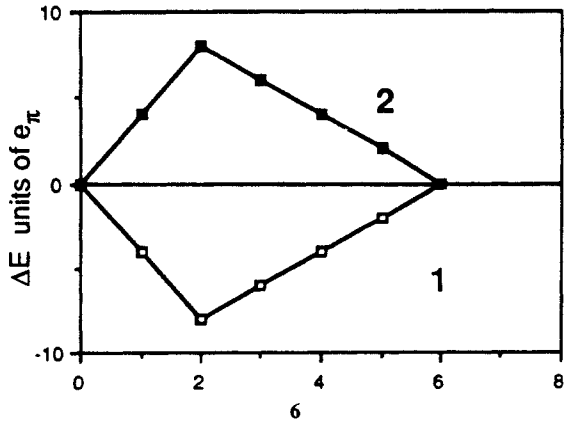

6

the mean-value point approximation. The result is in rather excellent agreement with the results from the tight-binding calculations of Figure 3. For the rutile structure of CrO_2, the d_{z^2} orbital projection from the total DOS has a significant contribution in the t_{2g} band as shown in Figure 7. It is this mixing, absent in the molecule, that so dramatically changes the shape of the energy difference curves.

We point out too that the O–O interactions also play a role in controlling the local geometry at the metal. We have emphasized their importance in our earlier study[15] on TiO_2, in which we suggested that the observed geometrical distortion in rutile TiO_2, case **2**, was directly due to the effect of such nonbonded repulsions. Structure **2** is favored at d^0 because of O–O repulsions, but **1** is favored for all other d counts because of the effect described above. VO_2 has a structure with a distortion in the same sense as that for TiO_2, but we believe our failure to get this structure correct in Figure 3 is the wrong weight our band structure calculations give for the two effects. However, there is a small change in the importance of these O–O effects as the d band is filled. With reference to Figure 4, the overlap between bridging O atoms along the chain axis with the axial atoms increases when the distortion is of the 2S + 4L type (**1**). In the t_{2g} levels this O–O interaction is nonbonding at the bottom of the band and bonding near the top, which stabilizes the observed geometry for later counts (d^4–d^6). Thus, the O–O repulsions that are influential in TiO_2 become slightly attractive in CrO_2, RuO_2, and OsO_2 and cause the energy differences at d^6 to be nonzero.

Structures of Rutile-Type Oxides and Fluorides

At this stage we can look at the larger picture for the rutile-type oxides and fluorides. The theoretical results we have emphasized above, and in our earlier work on anatase and rutile TiO_2, lead to a model where the actual ratio of r_2/r_4 (the ratio of the 2-fold set of distances to the 4-fold in the tetragonal structure) is determined by the interplay of anion–anion repulsions and electronic effects associated with the nature of metal–ligand bonding. There are two electronic effect to be considered here. Because of the geometry at the anion in the rutile structure, we expect to find two short and four long distances around the metal center. These ideas are cemented by results[15] of band-structure calculations on an undistorted rutile arrangement with all metal–oxygen distances equal. Two linkages have larger bond overlap populations (for all d counts) than do the other four. The second effect has been described in this paper, namely the driving force associated with the 2S + 4L situation for all d counts involving t_{2g} degeneracies.

For the fluorides the metal–anion distance is slightly longer than that in the oxides, but more importantly the nonbonded radius is smaller. Here, we expect anion–anion repulsions to be unimportant in determining the local geometry so that the electronic effects dominate. In accord with this idea $r_2/r_4 < 1$ for MgF_2 but > 1 for TiO_2, two d^0 systems. Other support comes from the large thermal motion observed for the metal in room-temperature diffraction experiments[15,32] on TiO_2 but its absence in the metal fluorides. For the fluorides in general therefore, both electronic effects favor a situation where $r_2/r_4 < 1$. The absence of any Jahn–Teller distorted structures with $r_2/r_4 > 1$ (as predicted for CoF_2 with the local model) suggests that electronic (covalent) effects are important here too. In other words, the label "typical ionic solids", which is often applied to rutile-type oxides and fluorides, is not an appropriate one.[33]

We have performed band-structure calculations on MF_2 fluorides (using the fluorine parameters given in the Appendix). The general shapes of the energy difference curves turn out to be quite similar to those shown for the oxides in Figure 4. It can be argued, of course, that such results are strongly dependent on the parameters used in the computations. We find in fact that, as the fluorine exponent is contracted to 2.600, not only do the

(32) (a) Baur, W. H. *Acta Crystallogr.* **1961**, *14*, 209. (b) Baur, W. H.; Khan, A. A. *Acta Crystallogr.* **1971**, *B27*, 2133. Baur, W. H. *Acta Crystallogr.* **1976**, *B32*, 2200.

(33) Elsewhere we show (Smyth, J.; Burdett, J. K., unpublished work) that the details of the rutile structure of TiO_2 may be reproduced not only with a model where the metal charge is set at +4 but also with a model where the metal charge is set to zero. See also: Burdett, J. K. *Chem. Rev.* **1988**, *88*, 3.

energy differences between structural alternatives become smaller but the shape of the energy difference curves become closer to those of **3**. Thus, in the fluorides there is the very real possibility that the overall picture is a balance between "local" and "extended" effects. There is some experimental evidence that points toward this state of affairs. It is interesting to note that a distortion of type **1** is found very strongly for FeF_2, a configuration where the energy is lowered on distortion by both local and extended mechanisms, but a much smaller effect is seen in CoF_2, where the local mechanism favors **2** but the extended mechanism favors **1**.

We can also see which distortion of the octahedron is predicted from the ionic model. Instead of performing Madelung calculations with the lack of insight that the computed numbers give us, we will use an idea of O'Keeffe.[34] He suggested that the lowest energy structure is the one of *maximum* volume, subject to the constraint of a fixed anion–cation distance, since here the anion–anion repulsions should be minimized. (Such a model naturally ignores the other terms in the energy, such as the cation–cation interactions.) In terms of the two distances around the metal atom the volume of the unit cell is given by eq 2. The

$$V^2 = (r_2^4/u^6)[r_4^2u^2 - (\tfrac{1}{2} - u)^2r_2^2] \quad (2)$$

change in this value on stretching r_2 and compressing r_4 in the way indicated in eq 1 is proportional to eq 3, which is positive if $u > 0.25$. This result is of course similar to the one we obtained

$$u^2 - (\tfrac{1}{2} - u)^2 \quad (3)$$

earlier for TiO_2, namely that the relief of anion–anion repulsions (whether of the ionic or covalent type) is best achieved in the 2L + 4S mode. An ionic model then encourages distortion in the opposite direction to that actually observed.

This experimental observation of the titanium atom "rattling" in the hole in the rutile structure indicates that the Ti–O distance should be somewhat shorter if anion–cation forces dominated the picture. It also leads us to ask whether tetrahedral coordination should be favored. The answer, difficult to quantify is that, for this d^0 metal, π bonding with the metal is especially good in the octahedral geometry.

(34) O'Keeffe, M. *Acta. Crystallogr.* **1977**, *A33*, 924.

The ideas described in this work have used one-electron molecular orbital theory. The crystal field theory has also been used to study molecular problems of this type.[35] Certainly, since the form of the splitting patterns of octahedral transition-metal energy levels are controlled purely by symmetry, the crystal field predictions as to the preferred route for these molecules will be similar to those obtained with the angular overlap model, although the distinction between π donors and acceptors does not exist on the crystal field model. In the extended solid the result we have shown in **5** involving mixing of the a_1 orbitals may be mimicked by the addition of a uniaxial field of judiciously chosen strength along the chain direction. We prefer to describe this structural problem by using the language of the covalent angular overlap model with its quantitative aspects associated with σ and π strengths rather than the comparatively vague ideas of the crystal field theory.

Acknowledgment. This research was supported by the National Science Foundation, by Grant (to J.K.B.) NSF DMR8414175, and by a grant through the Materials Research Laboratory at the University of Chicago (NSF DMR8519460). J.W.R. acknowledges support of the Intense Pulsed Neutron Source by DOE, Contract W-31-109-ENG-38. We thank J. D. Jorgensen and K. J. Volin of Argonne National Laboratory for use of the SEPD diffractometer and Dr. R. Kulkarni for performing some of the calculations. We are extremely grateful to Dr. Arthur Sleight and his group at Du Pont for the gift of a sample of CrO_2.

Appendix

The tight-binding calculations were performed along the lines of the earlier work[15] and with the same parameters for metal and oxygen. The parameters for fluorine were however (exponents in parentheses) the following: 2s, $H_{ii} = -40.00$ eV (1.245); 2p, $H_{2i} = -30.00$ eV (1.245).

Registry No. CrO_2, 12018-01-8.

Supplementary Material Available: Tables of time-of-flight and *d* spacing for CrO_2 at room temperature and 173 and 10 K (33 pages). Ordering information is given on any current masthead page.

(35) *Dunn*, T. M.; McClure, D. S.; Pearson, R. G. *Some Aspects of Crystal Field Theory*; Harper and Row: New York, 1965.

Vanadium Nitride Linear Chain Polymers and Monomers. Synthesis and Structures of $[V(\mu\text{-}N)Cl_2(py)_2]_\infty$ and $V(N)Cl_2(quin)_2$

Susan C. Critchlow, Megan E. Lerchen, Randal C. Smith, and Nancy M. Doherty*

Contribution from the Department of Chemistry, University of Washington, Seattle, Washington 98195. *Received November 20, 1987. Revised Manuscript Received June 2, 1988*

Abstract: A series of vanadium(V) nitrido complexes of formula $[V(N)Cl_2L_2]_n$ has been prepared by net loss of chlorotrimethylsilane from the vanadium(V) trimethylsilylimido trichloride, $Cl_3V{\equiv}NSiMe_3$, on reaction with substituted pyridines or an amine. For L = py or 4-Mepy, insoluble nitride-bridged linear chain polymers are produced. An X-ray structure of $[V(\mu\text{-}N)Cl_2(py)_2]_\infty$ reveals distorted octahedral vanadium centers joined by alternating short (1.571 (7) Å) and long (2.729 (7) Å) V–N bonds. In contrast, for L = 4-Etpy, 4-*t*-Bupy, or quinuclidine, soluble monomeric terminal nitride complexes are formed. The X-ray structure of $V(N)Cl_2(quin)_2$ indicates that this compound also possesses a monomeric five-coordinate structure in the solid state with a short (1.568 (19) Å) terminal metal nitride bond. The stability of the nitride bridge is discussed in light of the differences in structure and solubility in this group of compounds and in terms of the observed interactions involving the ancillary ligands in the solid-state structure of $[V(\mu\text{-}N)Cl_2(py)_2]_\infty$.

The development of synthetic routes to transition-metal-containing polymers is a critical prerequisite for study of these important new materials.[1-3] We are particularly interested in polymers based on a metal–nitrogen backbone, $[M(\mu\text{-}N)L_n]_\infty$.

0002-7863/88/1510-8071$01.50/0